ACKNOWLEDGMENTS

The authors wish to thank Professor E. R. Beringer and Dr. I. Rezanka for the design of various computer setups and programs, Professor J. O. Rasmussen for helpful discussions, and the technical staff of the accelerator for its cooperation.

†Work supported by the U. S. Atomic Energy Commission.

[1]D. G. McCauley and J. E. Draper, Phys. Rev. C 4, 475 (1971).

[2]G. M. Temmer and N. P. Heydenburg, Phys. Rev. 104, 967 (1956).

[3]N. P. Heydenburg, G. F. Pieper and C. E. Anderson, Phys. Rev. 108, 106 (1957).

[4]C. M. Lederer, J. M. Hollander, and I. Perlman, *Table of Isotopes* (Wiley, New York, 1967), 6th ed., p. 214.

[5]C. J. Toeset and A. H. W. Aten, Jr., Radiochimica Acta, 9, 55 (1968).

[6]J. Chaumont, E. Roeckl, Y. Nir-el, C. Thibault-Philippe, R. Klapisch, and R. Bernas, Phys. Letters, 29B, 652 (1969).

[7]T. A. Doron and M. Blann, Nucl. Phys. A161, 12 (1971).

[8]R. A. Warner and J. E. Draper, Phys. Rev. C 1, 1069 (1970).

PHYSICAL REVIEW C VOLUME 7, NUMBER 1 JANUARY 1973

Neutron-Nucleus Total and Inelastic Cross Sections: 900 to 2600 MeV/c*

Walter Schimmerling†‡
Princeton-Pennsylvania Accelerator, Princeton, New Jersey 08540,
and Department of Environmental Sciences, Rutgers – The State University, New Brunswick, New Jersey 08903

and

Thomas J. Devlin, Warren W. Johnson, and Kirby G. Vosburgh†
Physics Department, Rutgers – The State University, New Brunswick, New Jersey 08903

and

Richard E. Mischke§
Joseph Henry Laboratories – Princeton University, Princeton, New Jersey 08540
(Received 7 February 1972)

Total cross sections have been measured for neutrons on 16 targets: 12 selected elements, muscle-tissue-equivalent plastic, water, shielding concrete, and plastic scintillator. The momenta of the incident neutrons 900 to 2600 MeV/c were determined by time of flight. Overall uncertainties are of the order of 5%. The dependence of the total cross sections on the atomic weight of the targets can be approximated by an A^{β} law, where β varies with momentum from 0.72 to 0.84. The momentum dependence of the cross sections is found to be similar to that of neutron-proton cross sections. Results and similar analyses are also presented for total inelastic cross sections.

1. INTRODUCTION

This report discusses the details of a measurement of the momentum (P) and atomic-weight (A) dependence of neutron-nucleus total and inelastic cross sections for incident neutron momenta between 900 and 2600 MeV/c. The cross-section data in this momentum region[1-5] show a transition from the low-energy behavior which has been well documented[6-15] to the slowly falling momentum dependence characteristic of high energies.[16-20] The available experimental data have been supplemented by several approximate calculations.[21-24] They are based on Monte Carlo methods, using available nucleon-nucleon cross sections, and reasonable assumptions regarding the distribution of nucleons inside the nucleus. Analytical methods for calculating high-energy nuclear cross sections have also been developed.[25,26]

The dependence of the cross sections on the mo-

mentum of the incident particle at high momenta is very similar to that of the p-p and n-p total cross sections. However, the neutron-nucleon cross sections exhibit strong variation in their momentum dependence in the range of 900 to 2500 MeV/c,[27] where no single experiment has data sufficient in quantity to describe the mass and energy dependence investigated here.

This experiment was performed at the Princeton-Pennsylvania accelerator (PPA) using a beam which contained a broad spectrum of neutron momenta; the momentum of each detected neutron was determined by time of flight. The neutron detectors subtended a range of solid angles from the attenuator location to allow an extrapolation to zero solid angle. The neutral beam line and neutron detector were essentially the same as for a companion experiment which measured neutron-proton (np) and neutron-deuteron (nd) total cross sections.[27]

The results of this experiment are of interest for models of scattering on complex nuclei. Further, the tabulations and simple parametrizations have applications in radiation shielding and dosimetry.[28]

Several previous experiments[29-32] have studied total inelastic cross sections in this momentum range. We add a substantial number of such measurements.

2. EXPERIMENTAL METHOD

A. Total and Partial Cross Sections

The transmission of neutrons through an attenuator is described by the equation

$$T = I/I_0 = \exp(-n\sigma x), \tag{2.1}$$

where the attenuator is assumed to be thin (multiple collisions neglected) and T is the transmission, I is the transmitted particle flux, I_0 is the incident particle flux, n is the number of nuclei/cm^3 in the attenuator, σ is the cross section (cm^2), and x is the thickness of the attenuator (cm).

The transmission was measured by counting the neutron rate with and without the attenuator inserted in the beam. Data collection runs are thus referred to as attenuator "in" and "out" runs. The measured neutron transmission data were corrected for effects of finite beam and detector sizes, according to the requirements for "good-geometry" measurements.[33,34]

The normalization of the detected neutron rate was accomplished with indirect beam intensity monitors. Several scintillation-counter-telescope monitors were placed in the neutron beam. Each responded to a constant fraction of the neutron flux. Detectors of different sizes were used to determine the neutron transmission rate. The transmission for a given solid angle, Ω_j, subtended by the jth detector is then determined by

$$T_j = C_{ji} M_0 / C_{j0} M_i , \tag{2.2}$$

where C_{ji} and M_i (C_{j0} and M_0) denote the detector and monitor counts for an "in" ("out") run. The partial cross section is

$$\sigma_j = (1/nx)\ln(C_{j0} M_i / C_{ji} M_0) . \tag{2.3}$$

Four different-sized detectors were used simultaneously, and the range of solid angles was further extended by varying the attenuator-to-detector distance.

The detected particles consisted not only of the transmitted beam, but also of particles that interacted in the attenuator and were scattered into the solid angle subtended by the detector. Thus,

$$\sigma_j = \sigma_T - \int_{t_j}^{0} \frac{d\sigma}{dt}\, dt , \tag{2.4}$$

where σ_T is the total cross section, $(d\sigma/dt)$ is the differential cross section for all reaction channels, and t_j is the four-momentum transfer ($t_j = k^2\Omega_j/\pi$, where k = the c.m. momentum and Ω_j = the c.m. solid angle).

The total cross section was obtained by extrapolating the partial cross sections to zero solid angle (i.e., zero four-momentum transfer). The extrapolation method compensates for effects such as multiple nuclear scattering.[33] Details of the extrapolation parametrization and its interpretation are presented in Sec. 3D.

B. Experimental Beam Line

A plan view of the beam line is shown in Fig. 1. The neutron beam was produced by the 3-GeV proton beam of the PPA on a Pt target. The center line of the neutron beam was at an angle of 20.9° from the proton direction.

A 2-in.-thick Pb filter was placed in the beam approximately 3 ft from the synchrotron target to reduce the flux of γ rays. It was removed and inserted by remote control. A sweeping magnet 30 ft from the target removed charged particles from the beam. This magnet also generated a beam of negatively charged particles used for various tests. A second sweeping magnet at 87 ft from the target removed charged particles originating in the primary collimator.

The beam consisted primarily of neutrons and γ rays. The neutral K-meson contamination is estimated to be of the order 1 : 1000. The beam was defined by a 6-ft-long, 1.750 ± 0.002-in.-diam steel primary collimator built into steel and heavy concrete shielding 70 ft from the synchrotron. A

second steel collimator, 2.625 ± 0.002 in. in diam and 5 ft long, at 95 ft, was used to eliminate particles interacting in the primary collimator.

The attenuators were positioned on a movable platform ~106 ft from the target, and the detector was at ~111 ft from the target. The collimators, the attenuators, and the detector were coaxial to within $\pm\frac{1}{32}$ in.

C. Momentum Determination for the Neutrons

For this experiment, the PPA produced beam in ~1-nsec bursts separated by 67 nsec. The momentum of each detected neutron was determined by measuring its time of flight (TOF) between its source and the detector. A signal obtained at the time the neutron was produced was used as the start signal for a time-to-amplitude converter (TAC), and the neutron detection signal was used as the stop signal. The TAC output signal amplitude is proportional to the time elapsed between the two input signals. The TAC output pulses were stored in a multichannel pulse-height analyzer (PHA). The time scale corresponding to the PHA scale, and hence the TOF of the neutrons in any given channel was determined by calibrating the PHA in terms of known time delays (calibrated cables). Similar systems are described elsewhere.[35,36]

The origin of the time scale was established as the TOF of γ rays in the beam. The TOF of the neutrons was measured with respect to this origin. The velocity of a neutron, β_j, in units of the speed of light is given by

$$\beta_j = T_\gamma/(k_t Q_j + T_\gamma)\,, \tag{2.5}$$

where T_γ is the TOF of the γ rays (nsec), k_j is the scale factor (nsec/channel), and Q_j is the time delay of the neutrons with respect to the γ rays (PHA channels corresponding to detector module j). For a particle of mass M at momentum P_j, the momentum resolution can be calculated by

$$dP_j/P_j = (P_j/M)^2(\beta T_\gamma)^{-1} d(k_t Q_u)\,. \tag{2.6}$$

The timing resolution of the TOF system was 1.7 nsec full width at half maximum (FWHM) as determined from the γ peak in the TOF spectrum. The momentum resolution calculated using Eq. (2.6) was 2% for 900 MeV/c and 11% for 2500 MeV/c neutrons. A typical TOF spectrum is shown in Fig. 2.

There is an ambiguity in the TOF measurement, since slow neutrons in one burst may be overtaken by fast neutrons from the succeeding burst. With a 67-nsec interval between bursts, this occurs for neutrons of momenta below 750 MeV/c for the flight path used in this experiment. In order to discriminate against such neutrons a range cutoff was introduced in the detector. (See Sec. 2 F.)

D. Beam Monitors

There were four scintillation-counter telescopes in the neutral beam: G, J, W, and I as shown in Fig. 1. They differed in size, shape, rate, and response to neutron interactions in the beam. A comparison was made of their performance throughout the experiment, and temporary malfunctions in the monitors were detected and remedied. Section 3 B describes the method used to check the consistency of the monitors and to compute the normalization for a given subset of the data.

Also shown in Fig. 1 are two counter telescopes in the charged beams, S and X. These were used for various auxiliary functions such as checking

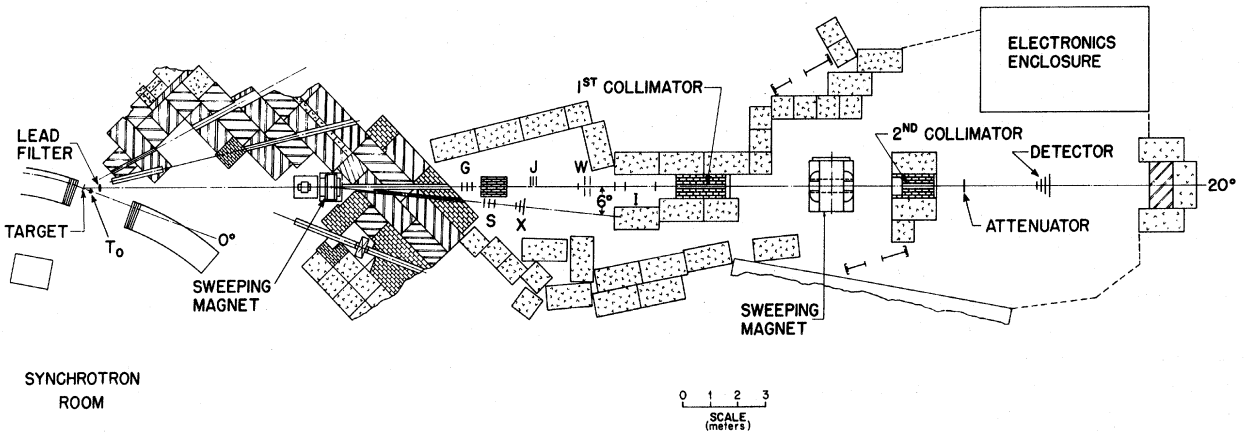

FIG. 1. Plan view of the experimental beam line. The various scintillation counters (G, J, W, I, S, X) are not drawn to scale.

TABLE I. Properties of the elemental attenuators.

Name	$1/nx$ (mb)
Beryllium	1597
Carbon	1776
Aluminum	3250
Iron	5612
Nickel	5856
Copper	6319
Zinc	6408
Silver	9852
Tin	10428
Lead	14143
Bismuth	14173
Uranium	16988

the stability of the TOF system but not for normalization.

E. Attenuators

The properties of the attenuators are listed in Tables I and II. The quantity $(1/nx)$ in Eq. (2.3) was obtained for each attenuator form

$$mx = \rho x A_0 / A , \tag{2.7}$$

where A is the atomic weight, A_0 is Avogadro's number, and ρ is density in g/cm^3.

For molecular targets, an average $\langle nx \rangle$ was calculated:

$$\langle nx \rangle = \rho x A_0 \sum_i p_i / A_i = \rho x A_0 \, (\sum_i m_i)/(\sum_i m_i A)$$
$$= \rho x A_0 / \langle A \rangle \tag{2.8}$$

where ρ_i is the fraction by weight of component i of the attenuator, and m_i is the number of atoms of each component per molecule. If the cross sections are weighted by the latter quantity, it is easy to show that

$$\langle nx\sigma \rangle = \sum_i n_i x \sigma_i = \langle nx \rangle \langle \sigma \rangle ,$$
$$\langle \sigma \rangle \equiv (\sum_i m_i \sigma_i)/(\sum_i m_i) . \tag{2.9}$$

We feel this to be a particularly convenient choice of weighted averages which should give an exact result for the attenuation in any substance.

The thickness of the attenuators was chosen for a value of $(n\sigma x) \simeq 0.2$ for all materials to give reasonable attenuation without large multiple scattering corrections. Experimental measurements confirmed that multiple nuclear collisions in the attenuator had a negligible effect on σ_T. (See Sec. 3 F.)

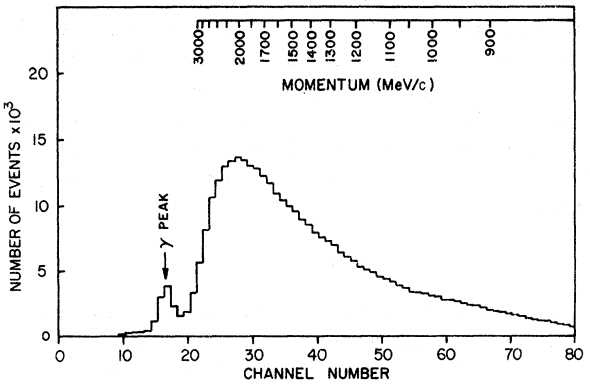

FIG. 2. A typical time-of-flight spectrum. The calibration is approximately 1 nsec/channel. The upper, nonlinear scale gives a momentum corresponding to the TOF channel number. The steep slope of the spectrum at high momenta amplifies the effects of any timing shifts. The data are shown before being grouped into bins as described in Sec. 3 C.

TABLE II. Properties of the molecular attenuators.

Name	Equivalent $1/nx$ (mb)	Composition (wt %)
Muscle-tissue-equivalent plastic A-150 [a]	1041	C: 77.3 H: 10.25 N: 3.49 O: 3.99 F: 2.44 Ca: 2.54
Pilot B scintillator [b]	798	C: 91.6 H: 8.4
LC240 concrete (Ilmenite) [c]	3812	Fe: 38 O: 32 Ca: 22 Si: 8
Distilled water	882	H: 11 O: 89

[a] Material and composition kindly provided by Professor Francis Shonka, Physical Science Laboratory, St. Procopius College, Lisle, Ill. 60532.

[b] Pilot Chemical Div., New England Nuclear Corp., 36 Pleasant St., Watertown, Mass.

[c] C. J. Tsao, R. B. Curtis, and G. K. O'Neill, Princeton-Pennsylvania Report PPAD-A45, 1958 (unpublished). The shielding material was manufactured to PPA specifications by various manufacturers.

The attenuator mounts were designed to minimize the material near the beam. The attenuators were glued between two sheets of 0.002-in.-thick Mylar. A similar mounting without an attenuator was inserted in the beam for the "out" runs. Longitudinal displacements of the attenuators to pinned positions along rails were used to vary the solid angles subtended by the neutron detector.

F. Neutron Detector

The neutron detector is shown schematically in Fig. 3. The scale has been expanded along the beam direction to separate the components. The detector was 24 by 24 in. in the plane perpendicular to the beam. It consisted of an initial counter A, followed by four modules (B, C, D, and E), $2\frac{1}{2}$ in. of steel, and a final counter F.

Each module contained three counters. The first counter (type "0") consisted of a 1-in.-thick Lucite disk-shaped converter centered and glued inside a rectangular Lucite box with walls $\frac{1}{8}$-in. thick. The converters were 5.0, 8.0, 10.3, and 12.0 in. in diam. The boxes were filled with a mineral-oil-based liquid scintillator[37] which was used to detect particles produced outside the converter. The second counter (type "1") was $\frac{1}{4}$-in.-thick circular plastic scintillator positioned in the center of a 24 by 24-in. Lucite spacer. The spacer was included so that the amount of material encountered by a neutron would be independent of the distance from the beam axis. The diam of these counters matched the converter. The third counters (type "2") were $\frac{1}{4}$ in. thick and a full 24×24 in. They were placed in coincidence with the solid-angle-defining counters and also served to detect charged particles incident on the next module. The A and F counters were also of this type.

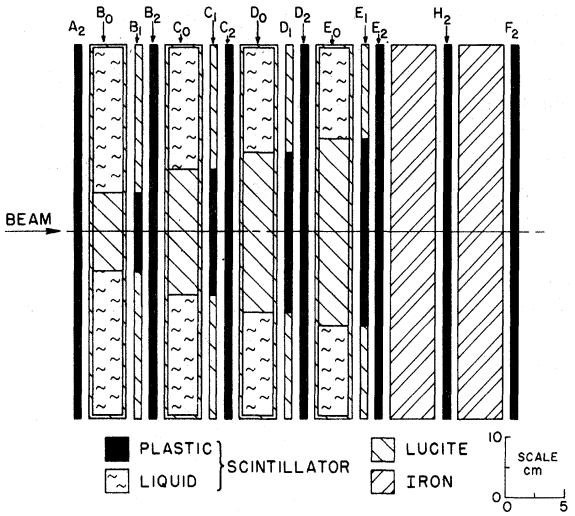

FIG. 3. The neutron detector. The various components of the first module are indicated as: B_0: Lucite neutron converter surrounded by liquid scintillator used to veto events outside the conversion volume; A_2, B_1, and B_2: plastic scintillators used to define the position of the conversion point. This pattern is repeated in the other modules. Note that the horizontal and vertical scales are different. The counter between the two steel slabs was not used in this work.

G. Electronics

The functions of the electronics in this experiment fall into several categories: (1) formation of the timing signal, T_0, which was produced when a burst of protons struck the production target; (2) formation of the timing signal originating in any one of the four transmission detectors; (3) processing and storage of the TOF information by a TAC and a PHA; (4) calibrations and checks of system performance; (5) processing and storage of monitor information.

The start signal for the TOF system was pro-

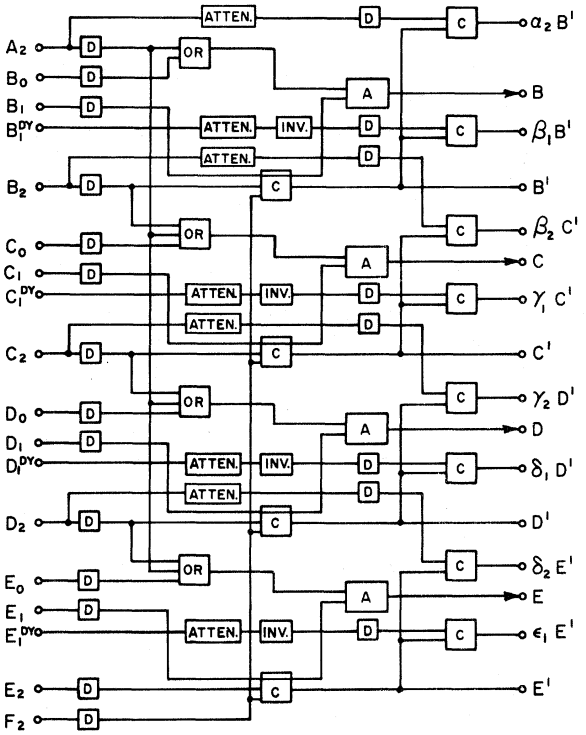

FIG. 4. Schematic of the detector electronics. The symbols are: D, fixed-threshold discriminator; C, coincidence; A, anticoincidence; ATTEN., attenuator; INV., inverter; o, scaler output; →, further connection to electronics not shown here.

vided by a signal (T_{01}) from a water Cherenkov counter placed near the synchrotron target. The T_{01} signal was fed into two discriminators: a fixed-threshold discriminator and a zero-crossing discriminator for time definition. The signals were placed in coincidence with the zero-crossing output delayed to determine the timing of the coincidence output. This output (T_0) was passed through a variable delay used for precise time adjustments and small corrections for drifts. Since T_0 was required before an event TOF could be recorded, appropriate coincidence logic was included to ensure that no event was processed which lacked a T_0 signal. The fraction of events with T_0 present was measured continuously and found to be about 98% with variations of order 1%. This introduced negligible error into the final cross sections, since monitors were corrected for T_0 inefficiency.

A block diagram of the neutron detector electronics is shown in Fig. 4. Valid neutron events were defined as (barred signals signify anticoincidence)

$$B = \bar{A}_2 \bar{B}_0 B_1 B_2 F_2 ,$$

$$C = \bar{A}_2 \bar{B}_2 \bar{C}_0 C_1 C_2 F_2 ,$$

$$D = \bar{A}_2 \bar{C}_2 \bar{D}_0 D_1 D_2 F_2 ,$$

$$E = \bar{A}_2 \bar{D}_2 \bar{E}_0 E_1 E_2 F_2 .$$

Counter F_2 was required to ensure that the charged interaction products had at least enough energy to penetrate the steel absorber, thus setting an energy threshold on the detected neutrons.

Coincidence timing was arranged to ensure that the start and stop signals to the TAC were always derived from T_0 and the appropriate "1" counter. The TAC output was sent to a 1024-channel PHA. The memory of the PHA was separated into eight 128-channel banks, each bank constituting a complete TOF spectrum. Each of the detector modules was assigned one bank. A fifth bank was used to store spectra from multiple-module events (usually events too closely spaced in time to be separated by the gating and routing logic). The other banks were used for periodic TOF calibration runs.

The monitor electronics were standard three-counter-telescope logic systems which were gated and scaled appropriately. Several auxiliary functions of the monitors are described in the next section.

A master gating system was used to turn on the fast logic only during a predetermined optimum interval within the synchrotron spill time. This interval was chosen to obtain uniform beam intensity and minimum variation of primary proton momenta. The system also gated off the electronics after each event was detected and kept it off for the duration of the PHA dead time.

H. Calibration and Checking Procedures

Detector Efficiency

The detector efficiency can vary due to changes in the gain of the photomultipliers and mechanical stresses in the scintillator and light-pipe assemblies. Temperature changes will cause variations in the behavior of the electronic components which appear as effective changes in efficiency; they may also be the source of mechanical stresses.

The temperature of the electronics enclosure was kept constant using air conditioning and fans. The detector was enclosed and maintained at constant temperature by cool air piped in from the electronics enclosure.

Each photomultiplier was operated well into its voltage plateau in order to have minimum dependence on drifts in the high voltage and to have optimum efficiency. The voltages were monitored throughout the experiment and all observed changes were smaller than 0.1%.

Auxiliary signals were derived from "1" and "2" counters to monitor the counter efficiency, as shown in Fig. 4. These signals were attenuated and placed in coincidence with the "1" and "2" counters of each module together with the F signal. These signals are $\alpha_2 B'$, $\beta_2 C'$, $\gamma_2 D'$, $\delta_2 E'$, $\beta_1 B'$, $\gamma_1 C'$, $\delta_1 D'$, and $\epsilon_1 E'$. The attenuation was chosen to correspond to the 50% point in photomultiplier gain. In addition, the relative counting rates for each of the four modules were recorded and compared (B', C', D', and E'). Some discontinuous changes in the relative efficiencies were found for groups of runs, mainly in the efficiency of E, the largest of the detector modules. These changes could not be traced back to any single cause. They may be due to occasional temperature variations which are known to have occurred. The data from a module showing an abrupt variation in efficiency were excluded from the partial cross-section data set for the affected runs.

Time-of-Flight Calibrations and Stability

The PHA time scale was calibrated by removing the Pb filter from the beam and taking TOF spectra where the γ rays dominated. Two spectra were taken for every calibration, one without additional delays, and one with T_0 delayed by a calibrated 78.35-nsec delay. The first spectrum defined the origin of the time scale as the position of the γ peak, while the combination of both gave

the number of PHA channels corresponding to 78.35 nsec. This gave a value for the quantity k_t in Eq. (2.5), equal to 0.850 ± 0.002 nsec/channel.

The functioning of the TAC and the linearity of the TOF system were checked using a pulse generator as the event signal. Since there was no correlation between the pulses from the generator and T_0 pulses, a uniform distribution of time intervals, or "white spectrum" resulted. Nonlinearities in the analyzer found in this way amounted to less than 0.1%.

Drifts in T_0 timing were monitored using a "time vernier" described in detail in Ref. 36. The system was sensitive to changes of 0.1 nsec.

Alternate Bucket Contamination

The operating mode of the PPA which gives 67-nsec intervals between proton bursts in achieved by electrostatic chopping at injection. This results in filling only four of the eight phase-stable regions (buckets). Normally, the number of protons in the "empty" buckets is less than 0.1% of the number in the "full" buckets. At this level, the background of unwanted events from "empty" buckets in negligible. However, unexpected changes in synchrotron tuning can raise this "alternate bucket contamination" to undesirable levels. The S monitor was used to monitor the alternate bucket contamination. To do this, an ST_0 coincidence was set up between the S monitor and T_0 and compared with the same coincidence obtained by delaying T_0 33 nsec. The alternate bucket contamination remained less than the noise level of 0.1% for the duration of the experiment.

Intensity Variations

The synchrotron magnet program at the PPA is sinusoidal. This causes a 10% variation in proton momentum during the beam spill time. Variations in the spill rate as a function of spill time and thus as a function of proton momentum were monitored using the X telescope. The X monitor counts were separated into four spill-time regions and recorded separately on four scalers using timing signals from the synchrotron to gate a signal correlator. The four relative counting rates remained in constant proportion within tolerable limits.

I. Solid Angle Correction

The efficiencies of the detector modules were not uniform over their full area due to geometrical edge effects. For a neutron striking the edge the relative efficiency should be about 50%, since the recoil proton has an equal probability of going away from or toward the axis of the detector. (Multiparticle final states raise the edge efficiency.) The rate of spatial variation of the relative efficiency depends on the angular distribution of the recoil protons in the laboratory system. This nonuniform relative efficiency can be accounted for by defining an "effective solid angle," since the average detecting surface is smaller than the detector area when weighted in this manner. This definition applies to the scattered neutrons; the efficiency for the transmitted beam does not change from "out" to "in" measurements. It also assumes a uniform flux of neutrons.

The radial dependence of the relative efficiency can be measured by moving the detector across the beam. With a pencil beam the relative efficiency is directly measured in this manner. We performed such a measurement with reduced apertures in the neutron beam. The resultant efficiency profiles were used to compute the "effective" solid angles used in the analysis.

J. Data Collection

Data were taken at two detector positions: 110.7 and 118 ft from the synchrotron target, and a total of four attenuator-to-detector distances: 30.9, 60.4, 117, and 204 in. (±0.1 in.). In addition a few runs were taken at an attenuator-to-detector distance of 16.4 in. in the first detector position.

Approximately two million events were detected in each "in" run for a given attenuator and one detector position. The attenuator was then changed and a new run started. Each run took $\sim 1\frac{1}{2}$ h. An "out" measurement and a γ peak calibration were performed for every three "in" runs.

A total of 272 runs were performed, of which 50 correspond to testing and debugging of the apparatus, and were discarded. For each run the TOF spectra were punched on paper tape and typed. The recorded scaler data consisted of monitor telescope counts, integrated events per module, total number of events (with and without T_0 coincidence), detector efficiency monitoring signals, relative proton beam intensity, and time-vernier coincidence rates. Other data for each run consisted of scaler counts, attenuator parameters and position, T_0 delay, and beam status data such as magnet currents and γ-filter position. All the run data were transferred to magnetic tape for computer processing and checked against the original records.

3. DATA ANALYSIS

A. Data Selection

To group runs in a systematic way, the long-term variation of relative monitor counts, events

TABLE III. Total neutron-nucleus cross sections (mb).

Momentum bin (MeV/c)	P_{av} (MeV)	T_{av} (MeV)	Be	C	Al	Fe	Ni	Cu	Zn	Ag	Sn	Pb	Bi	U
900–950	925	379	254±8	299±8	571±19	1024±29	1132±24	1174±33	1284±44	1786±43	1993±63	2769±78	3043±111	3071±80
950–1000	975	414	250±9	287±8	564±18	987±29	1130±23	1088±31	1251±28	1870±56	1951±61	2765±75	2932±106	3112±77
1000–1050	1025	451	262±9	317±8	589±18	1035±29	1105±23	1134±31	1309±42	1850±55	1897±60	2864±75	3138±103	3162±76
1050–1100	1075	488	252±9	317±8	570±18	1067±30	1155±23	1174±32	1269±42	1781±56	1969±60	2732±76	2929±104	3163±78
1100–1200	1150	545	273±6	333±6	632±14	1107±25	1184±17	1169±24	1387±33	1907±42	2070±46	2929±61	3067±87	3309±59
1200–1300	1250	624	282±5	328±6	640±14	1073±27	1192±17	1186±24	1356±32	1920±42	2029±45	2880±59	3135±78	3167±60
1300–1400	1350	705	295±7	350±6	667±15	1126±26	1241±18	1243±24	1480±34	1981±43	1981±46	2897±62	3097±79	3232±63
1400–1500	1450	788	293±8	353±6	687±16	1114±27	1227±18	1300±25	1398±34	1859±44	2044±48	3017±65	2998±81	3274±66
1500–1600	1550	873	290±8	351±7	688±17	1142±29	1204±20	1264±26	1412±35	2033±47	2073±51	3074±70	3041±86	3239±72
1600–1700	1650	959	290±8	358±7	704±18	1181±31	1266±21	1331±28	1431±37	1974±50	2119±55	3091±77	3182±92	3340±77
1700–1850	1775	1069	307±8	352±7	689±17	1142±31	1235±19	1245±25	1397±34	1887±46	2025±50	3016±72	3028±85	3179±72
1850–2000	1925	1202	313±8	380±7	674±19	1159±32	1272±20	1303±28	1436±37	1910±50	2179±54	3139±79	3090±92	3452±79
2000–2200	2100	1361	314±8	364±7	725±19	1180±32	1261±19	1304±26	1370±35	1896±47	1952±51	3092±78	3072±89	3448±78
2200–2400	2300	1545	308±9	363±8	718±23	1134±35	1254±22	1306±31	1359±39	1942±55	2151±61	3189±93	3091±106	3378±93
2400–2600	2500	1731	321±13	408±12	797±35	1095±50	1289±33	1367±46	1419±56	1813±85	1920±93	3003±144	2735±163	3637±144
Scale uncertainty (mb)			±15	±9	±16	±27	±32	±33	±72	±50	±53	±78	±80	±85

per module, efficiency monitors, and γ-peak positions were studied. In addition to obvious malfunctions noted during the experiment, it was found that: (1) Long-term drifts existed in the relative proportion of monitor counting rates; (2) long-term drifts existed in the position of the γ peaks, and short-term drifts were of the order of 0.1 nsec or less between γ calibrations; (3) occasional abrupt changes in a module's efficiency occurred as described in Sec. 2H, extending over several runs in some cases.

In order to take advantage of existing computer programs,[27] the data were grouped into "sets" containing two "in" runs and a common "out" run. The criteria for selecting the runs to be combined into a set were: (1) No known significant changes occurred in the time during which all the data in the set were taken; (2) the runs were all taken within an 8-h period to minimize the effect of drifts; (3) the results of the normalization procedure to be sescribed in Sec. 3 B yielded an acceptable fit.

The total amount of data rejected at the various stages of the analysis did not exceed 12% of the data taken.

B. Normalization

Data from each of four monitor telescopes were present for each of the three runs in a given data set. These 12 numbers were subjected to a least-squares fitting procedure in order to determine the best normalization ratios [M_i/M_0 in Eq. (2.2)]. Data in which there were obvious monitor malfunctions were discarded. Further tests were made on the basis of the χ^2 probability, P, in the normalization procedure. In cases where P was less than 1%, we attempted to improve the data by discarding one or more monitors or runs from consideration. In three cases a different "out" run was substituted. In about 5% of the cases P remained less than 1%, and these sets were discarded. About 25% of the cases had P between 1% and 10%. For these, the monitor variances were scaled up by a factor of χ^2/NDF.[38] (NDF is number of degrees of freedom.) The remaining 70% were accepted without adjustment of the normalization. Several sets consisting entirely of accepted "out" runs were also generated. The partial cross sections for all such sets, calculated as described in Sec. 3 C, were zero within statistical errors. This result indicates that no bias was introduced by the above process in selecting "out" runs.

Detector counting statistics dominate the errors, and uncertainties in the normalization error discussed above introduce a negligible effect. However, the final cross sections seem to fluctuate

from subjectively "smooth" curves more than one expects statistically, and in a way which suggests monitor fluctuations. In our judgment, one should assume an additional 4% uncertainty in element-to-element comparison. This should be interpreted only as an over-all scale uncertainty in the cross section vs momentum for a given element.

C. Calculation of Partial Cross Sections

The partial cross sections defined in Sec. 2 were calculated using Eq. (2.3). The neutron momenta were grouped into 17 intervals or "bins" consistent with the momentum resolution (see Table III) for all but the highest momentum, which has as its upper limit our high momentum cutoff. Partial cross sections were obtained for every module and every momentum bin, resulting in a total of between 12 and 20 partial cross sections for every attenuator, per momentum bin. Partial cross sections corresponding to the same solid angle and attenuator were averaged before being used in the solid-angle extrapolation.

D. Extrapolation Procedure

In principle, $d\sigma/dt$ in Eq. (2.4) can be separated into an elastic and an inelastic part. To a good approximation the elastic cross section is known to follow an exponential law of the type $a_1 \exp(-a_2 t)$ for small values of t.[39] In terms of an optical model for diffraction around a black disc,[40] $a_1 = \sigma_T/16\pi$ and $a_2 = \frac{1}{4}R^2$, where R is the nuclear "radius." The inelastic differential cross section was assumed to be isotropic, $d\sigma/dt_{\text{inel}} = a_3$. The total cross section was obtained by fitting the partial cross sections to a function of the form

$$\sigma_i = b_1 \exp(-b_2 t_i) + b_3 t_i + b_4 . \tag{3.1}$$

Comparison of Eq. (3.1) with Eq. (2.4) and the definitions a_1, a_2, and a_3 shows that $b_1 = a_1/a_2$, $b_2 = a_2$, $b_3 = -a_3$, and $\sigma_T = b_1 + b_4$.

Several constraints were imposed on the fitting function in order to attempt a physical interpretation of the coefficients in Eq. (3.1). It is clear that b_1, b_2, and b_4, as defined, must be positive, and that b_3 must be negative. The requirement on b_1 and b_4 stems from their interpretation in terms of the total elastic and inelastic cross section, while the requirements on the other two coefficients stem from the fact that the partial cross sections decrease with increasing t (i.e., the slopes must always be negative). These constraints were incorporated into the fitting program. In addition, the nuclear radius parameter was fixed according to

$$b_2 = 6.42 r_0^2 A^{2/3} \ (\text{GeV}/c)^{-2} , \tag{3.2}$$

where $r_0 = 1.27 \times 10^{-13}$ cm from a fit to high-energy nucleon-nucleus scattering data,[41] and the numerical factor is $(4\hbar^2 c^2)^{-1}$.

In the framework of the optical model (disregarding spin), the dimensionless quantity $b_4/b_2 = 4\pi$. This equality cannot be expected to hold exactly due to the limitations of the model. However, it was roughly constant with momentum for each target, confirming that the fitting procedure was reasonable.

The extrapolated cross sections are extremely insensitive to the specific fitting function. Various trial fitting functions were tried in the early stages of the data analysis: parabolic in t, simple exponential, and Eq. (3.1) without fixing b_2 to a given value, as well as changing b_2 by factors of 2. The total cross sections so obtained did not differ by more than 1 standard deviation from each other, although some of the fits were noticeably worse than others.

The partial cross sections were extrapolated using a computer program[38] to minimize χ^2 given by

$$\chi^2 = \sum [\sigma_i - f(b)] W_{ij}^{-1} [\sigma_j - f(b)] , \tag{3.3}$$

where $f(b)$ is the function given by Eq. (3.1), and W_{ij} is the input data weight matrix. The values of the minimum χ^2 were on the average equal to NDF.

Two sources of random error were considered: event counting statistics and monitor normalization. The normalization uncertainties gave rise to module-to-module correlations, since the same normalization parameter was used for all four modules in a given run. It was assumed that there were no correlations among module events or between monitors and modules.

In the extrapolation to zero angle, the parameter errors, as well as the statistical errors in the total cross sections, were obtained from the parameter error matrix V^{-1}, where

$$V_{ij} = \frac{1}{2} \frac{\partial^2(\chi^2)}{\partial b_i \partial b_j} \tag{3.4}$$

and the b's are the fitting parameters.[42]

E. Backgrounds

A low momentum neutron background was present in the TOF spectrum region corresponding to the highest momentum bins. This background contributed less than 0.5% to the B and C modules, but between 1 and 2% of the D and E modules. The affected data were discarded.

The effect of accidental coincidences were assessed in a subsequent experiment,[27] after the additional counter shown in Fig. 3 was inserted in the steel. The effect of accidentals was estimated to be of the order of 1% of the partial cross sections.

F. Systematic Effects

The following sources of systematic uncertainties do not contribute significantly to the final errors (~0.1% each): (1) errors in the determination of the flight path for the neutrons, (2) nonlinearities in the PHA, (3) the alternate bucket contamination, and (4) contamination of the beam by neutral K mesons.

The following possible sources of nonnegligible systematic errors were considered:

Monitor drifts and fluctuations. As discussed in Sec. 3 B, we estimate run-to-run systematic fluctuations which behave like monitor errors. These errors affect the smoothness of the dependence of cross section on atomic weight for any given momentum, but do not affect the momentum dependence for a given element. The estimated magnitude of the uncertainty is 4% of the cross sections.

Timing drifts. There are two possible kinds of timing drifts: shifts in the origin and changes of the time scale. These may result in two types of errors: (1) mislabeling of momenta and (2) incompatible "in" and "out" pairs of runs. Short-term drifts of the origin corresponding to single data sets of three runs are estimated to be less than 0.1 nsec. The effect of such a shift is less than 2% up to a momentum of 2.6 GeV/c. This uncertainty was taken into account by adding the timing uncertainty in quadrature to the statistical uncertainties.

A systematic rate dependence of the TAC output was discovered subsequent to this experiment. As a result the scale factor k_t in Eq. (2.5) could vary between two values differing by approximately 1% corresponding to two states of the TAC. The estimated error due to this change of scale is as large as 10% for high momenta but less than 1% for momenta less than 2.6 GeV/c. The reason for this momentum dependence is the fact that higher momenta correspond to the steep slope portion of the TOF spectrum, as may be seen in Fig. 2. Very small changes in the time axis will be amplified greatly on the event axis. For this experiment, data above 2.6 GeV/c were discarded.

Variations in detector efficiency. These were detected as abrupt variations in the relative counting rates, which were constant within statistics during the rest of the experiment. Rather than correct the affected partial cross-section points, they were excluded from the fitting procedure. The elimination of such points improved the χ^2 of the fit.

Multiple nuclear collisions. Deviations from an exponential attenuation law due to multiple nuclear collisions in the attenuator were tested experimentally by measuring the transmission of Al attenuators in the range 0.1 to 0.4 mean free paths. A straight line fit was made to the partial cross sections, since only four solid angles existed for each Al thickness. The results have been plotted for representative momenta in Fig. 5. It may be seen that they are consistent with the assumption of a constant cross section and that multiple collisions do not affect the final results. A similar conclusion may be drawn for all attenuators, since their transmissions were approximately equal.

Target composition. The uniformity of the elemental targets and water was approximately 0.1% as determined by density measurements on different samples of the attenuator material. Only one sample of scintillator was measured. The estimated uncertainty was 1%. The uniformity of the other molecular attenuators determined in the same way was between 3 and 5%. The range in variation of the composition of the various molecular attenuators is estimated to be between 5 and 10%. The final uncertainty affects the average atomic weight

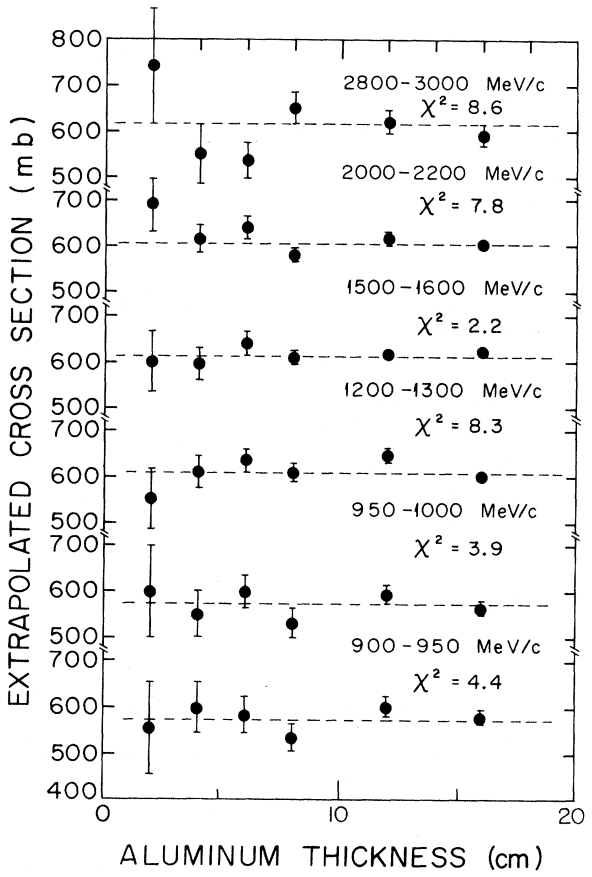

FIG. 5. The cross sections for aluminum as a function of attenuator thickness. Since there is no systematic dependence on thickness, we conclude that the double scattering correction is negligible. Values of χ^2 refer to comparisons of the dashed lines with the data.

of these attenuators at an estimated 7% level. These percentage errors affect the cross sections directly through the factor $1/nx$ in Eq. (2.3).

Summary of systematics. For the elemental targets water and scintillator, the unexplained 4% fluctuations which we have attributed to monitor errors dominate. For the other molecular attenuators, the 7% uncertainties in density and composition dominate.

4. RESULTS AND DISCUSSION

A. Total Cross Sections

The total cross sections for nuclear attenuators have been tabulated in Table III, together with their uncertainties. Also indicated are the momentum bin limits, the average momentum P_{av}, and the average kinetic energy T_{av} of the incident neutrons. The total cross sections were obtained by the extrapolation procedure described in Sec. 3D. Figure 6 shows the partial cross sections and fitted curves for nickel at several momenta to illustrate this procedure.

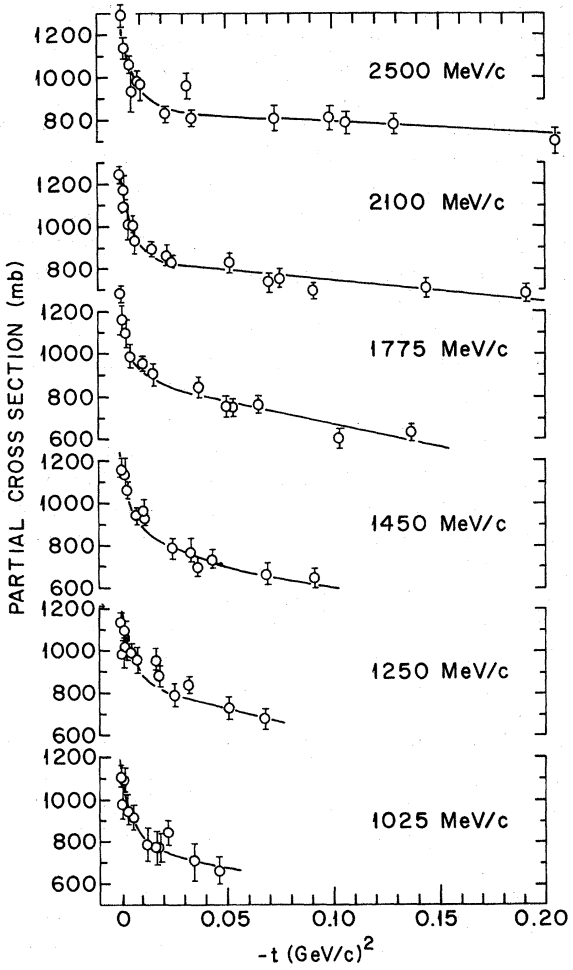

FIG. 6. Examples of the graphs for extrapolation to zero scattering angle. The independent variable, t, is the four-momentum transfer for an elastically scattered neutron which intersects the edge of the transmission counter. Note that the left-hand vertical axis is displaced from zero for clarity of presentation. The data presented are for Ni.

The uncertainties quoted with each cross section are determined mainly by counting statistics with the uncertainty due to timing shifts added in quadrature. Where correlations among these uncertainties exist, they are small. The over-all scale uncertainty for each element has been quoted separately. The scale uncertainties are fully correlated for cross sections at all momenta for a given element, but uncorrelated from element to element. There is probably an additional systematic error in the data for all elements at 2500 MeV/c. These data had the poorest momentum resolution and were most affected by timing drifts. From results of the fits described below, it may be of order 10–15%.

The total cross sections for neutrons on nuclei for incident momenta below 960 MeV/c have been discussed by Nedzel[2] and Ashmore *et al.*[1] A common feature of these cross sections is a rapid drop from their maximum value near the thresholds of nuclear reactions to minima at a momentum of approximately 800 MeV/c, the threshold for meson production.

The present measurements link the low-momentum region discussed above to the high-momentum

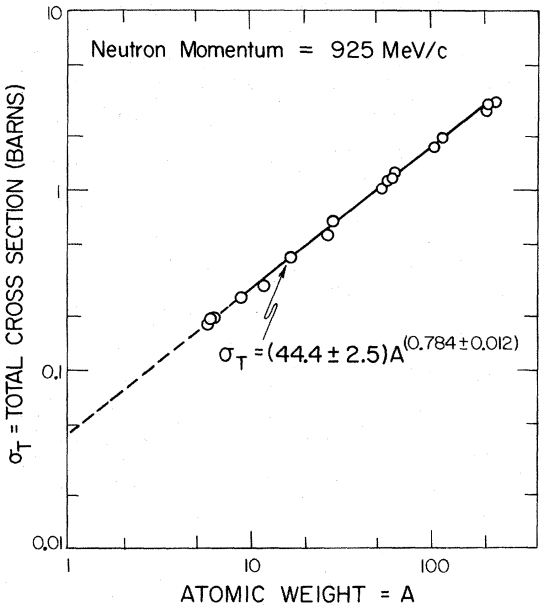

FIG. 7. Total cross sections as a function of atomic weight for 925 MeV/c.

TABLE IV. Neutron-nucleus total inelastic cross sections (mb).

Momentum bin (MeV/c)	P_{av} (MeV/c)	T_{av} (MeV)	Be	C	Al	Fe	Ni	Cu	Zn	Ag	Sn	Pb	Bi	U
900–950	925	379	168±40	268±45	490±55	757±65	685±60	775±149	734±212	1105±71	1013±252	1923±117	2437±725	2332±157
950–1000	975	414	179±98	261±38	476±47	814±59	786±53	926±126	875±120	967±260	947±216	1718±104	2538±595	2182±140
1000–1050	1025	451	205±86	242±32	486±42	834±53	791±48	1004±110	761±154	1230±225	1228±190	1840±94	1586±505	2104±130
1050–1100	1075	488	289±77	233±28	464±38	772±51	795±45	933±99	915±138	1191±201	1077±172	1753±88	2180±445	2157±123
1100–1200	1150	545	194±28	210±18	435±27	816±35	808±31	805±63	787±138	1022±124	1055±110	1579±101	1757±543	2269±88
1200–1300	1250	624	171±10	248±15	461±24	856±32	846±28	914±54	830±76	1069±104	1193±95	1857±54	2171±222	2278±81
1300–1400	1350	705	205±37	260±13	440±21	896±29	897±26	783±48	786±96	1169±90	1339±84	1853±51	2288±186	2240±76
1400–1500	1450	788	200±32	242±11	449±21	818±28	852±24	720±42	817±59	1328±80	1316±77	1784±48	2271±160	2182±72
1500–1600	1550	873	202±29	259±10	452±19	825±28	906±24	869±41	874±56	1143±75	1172±73	1802±47	2117±146	2298±70
1600–1700	1650	959	272±27	261±10	436±18	884±30	844±23	824±38	932±54	1261±70	1152±70	1783±47	2031±136	2330±69
1700–1850	1775	1069	216±30	268±9	450±16	840±23	887±19	819±32	848±44	1151±57	1244±57	1799±40	2162±108	2319±60
1850–2000	1925	1202	211±19	255±8	473±14	786±25	839±21	791±30	909±42	1176±53	1195±54	1815±39	2295±100	2319±59
2000–2200	2100	1361	178±15	258±6	483±13	805±19	843±17	784±25	979±37	1191±44	1352±45	1861±35	2085±80	2291±50
2200–2400	2300	1545	218±14	268±6	461±12	824±20	836±17	837±26	942±38	1332±44	1338±46	1899±36	2228±81	2337±52
2400–2600	2500	1731	221±19	251±8	472±16	816±28	850±24	766±40	995±50	1305±59	1305±63	1921±50	2238±105	2179±70
Scale uncertainty (mb)			±15	±9	±16	±27	±32	±33	±72	±50	±53	±78	±80	±85

region. Figure 2 of Schimmerling *et al.*[43] showed the total cross sections as a function of incident neutron momentum for momenta up to 20 GeV/c. Data from the most recent measurements in this range are also shown in that figure along with np and nd cross sections.[27,44-47] It may be seen that the total cross sections increase from a low value at ~800 MeV/c to a broad maximum around 2.3 GeV/c, decreasing slowly thereafter as a consequence of the decreasing nucleon-nucleon cross sections. The momentum dependence of the total cross sections is discussed in another context by Ericson and Locher.[48]

The momentum dependence of the total cross sections is similar to that of the np total cross sections in the present momentum range.[27] At higher momenta the ratio of the n-nucleus total cross sections to the np total cross section has been found to be constant for a given target nucleus between 8 and 21 GeV/c.[19] Interpretations of this behavior have been given elsewhere.[43,49,50]

The total cross sections for all attenuators have been plotted as a function of atomic weight in Fig. 7 for 925 MeV/c. The cross section for oxygen has been calculated using the results for water and the data for hydrogen from Ref. 27. The molecular attenuators have been plotted at a position corresponding to their average atomic weight as given by Eq. (2.8). To a first approximation the data are well represented over the experimental momentum range by a function of the form $\sigma_T = \sigma_0(P)A^{\beta(P)}$, where σ_0 and β are constants for a given momentum. The results are presented in Figs. 8 and 9. The quoted scale uncertainties were added in quadrature to the uncertainties on individual data points for the fits at each momentum. The fact that the values of χ^2 are generally acceptable indicates that our estimates of systematic uncertainties are correct. All elements from Table I were included in the fit ($9 \leq A \leq 238$).

The dependence of the total cross section on atomic weight does not support the assumption $\beta = \frac{2}{3}$ often made for calculations of nuclear cross sections.[51] Such cross sections used are between 10 and 25% smaller than the present experimental results, depending on element and momentum.

There is a statistically significant energy dependence in both parameters. As expected, $\sigma_0(P)$ has the same qualitative behavior as the elementary neutron-nucleon cross sections. The parameter $\beta(P)$ is observed to decrease with increasing elementary cross sections. To some approximation, the mean free path in nuclear matter should be inversely proportional to some weighted average of the elementary cross sections. If the mean free path is long compared to the nuclear diameter, we expect to have $\beta = 1$ and σ_0 small. If the mean

free path is very short, we expect complete shadowing with $\beta = \frac{2}{3}$ and σ_0 approximately equal to the prediction of a black sphere model. Since the same forces are responsible both for nuclear binding and the scattering process under study, it is not surprising that our results lie between the two extremes, and that they vary in a manner consistent with *np* and *nn* cross sections. These results supersede the preliminary analysis of the slope parameter, β, presented in Ref. 44.

B. Interpretation of the Extrapolation Parameters

The interpretation of the model used to fit the partial cross sections is that b_1 is the total elastic cross section and b_4 is the total inelastic cross section. Due to negative correlations the data do not constrain b_1 and b_4 separately, although their sum is well determined. These uncertainties due to these correlations are worse for light nuclei and for small momenta for the incident neutron, where only a small range of 5 is sampled, and where the "elastic" and the "inelastic" slopes may not be very different.

In those cases where the region extending beyond the first minimum in the diffraction peak is well sampled, mainly for momenta above 1100 MeV/c and for medium to heavy elements, the parameters can be used to obtain an estimate of the elastic and inelastic total cross sections. As an illustration, b_4 has been plotted as a function of incident neutron momentum in Fig. 10. Experimental values of inelastic cross sections have been included for comparison, using both *p*-nucleus and *n*-nucleus data. Also included are results from Monte Carlo

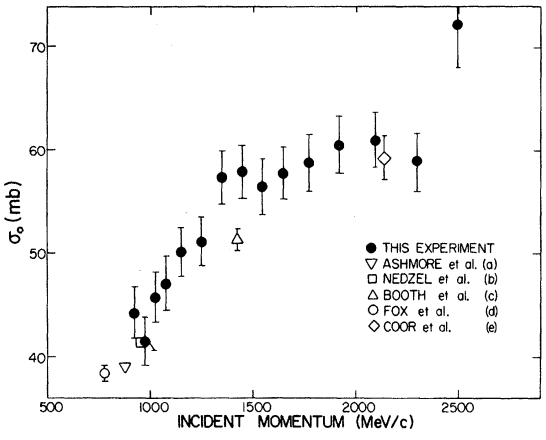

FIG. 8. The parameter $\sigma_0(P)$ as a function of momentum: (a) A. Ashmore *et al.*, Proc. Phys. Soc. (London) A70, 745 (1957); (b) V. Nedzel, Phys. Rev. 94, 174 (1954); (c) N. Booth *et al.*, Proc. Phys. Soc. (London) 71, 293 (1958); (d) R. Fox *et al.*, Phys. Rev. 80, 23 (1950); and (e) T. Coor *et al.*, Phys. Rev. 98, 1369 (1955).

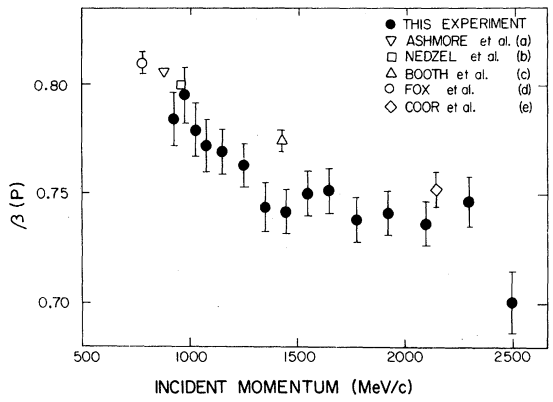

FIG. 9. The parameter β as a function of momentum. See Fig. 8 for symbols and references.

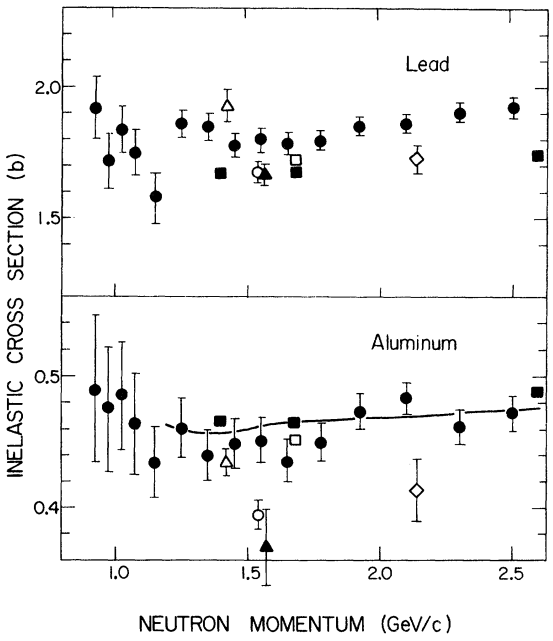

FIG. 10. The parameter b_4 for Al and Pb. The symbols are: □: neutrons and ■: protons, H. W. Bertini, Oak Ridge National Laboratory Reports Nos. ORNL-TM-1225, 1965 and ORNL-TM-1966, 1967 (unpublished); △: neutrons, N. E. Booth *et al.*, Proc. Phys. Soc. (London) 71, 293 (1958); ▲: protons, N. E. Booth *et al.*, Proc. Phys. Soc. (London) 71, 209 (1958); ●: protons, F. F. Chen *et al.*, Phys. Rev. 99, 857 (1955); ◇: neutrons, T. Coor *et al.*, Phys. Rev. 98, 1369 (1956); ○: neutrons, this experiment; and ___: D. V. Bugg *et al.*, Phys. Rev. 146, 980 (1966). This curve has been drawn from numbers obtained by subtracting the elastic from the total cross section in the graph of the original publication, and it has large, unknown uncertainties.

calculations by Bertini[23] of the penetration of protons and neutrons into nuclei. The agreement with other experimental data is surprisingly good, and b_1 and b_4 may be concluded to provide at least qualitative information on the components of the total cross sections.

Under the assumption that b_4 is a good measure of the total inelastic cross section, we present the results in Table IV. The uncertainties have the same interpretation as those in Table III. The magnitude of the scale uncertainty for each element is identical in magnitude and fully correlated with that given in Table III.

We have performed least-squares fits of the inelastic cross sections to the function

$$\sigma_I = \sigma_{0I}(P) A^{\beta I(P)} .$$

We find no statistically significant momentum dependence. The data at all momenta were subjected to a least-squares fit to a single pair of parameters. Correlated uncertainties were included in the calculation of χ^2. The results are

$$\sigma_{0I} = 43.2 \pm 2.3 ,$$

$$\beta_I = 0.719 \pm 0.012 ,$$

$$\chi^2 = 231 \ (\mathrm{NDF} = 178) .$$

The value of χ^2 is somewhat high. We attribute this to additional systematic errors in computing the inelastic cross section rather than to momentum dependence because χ^2 is not greatly improved by allowing the parameters to vary with momentum. Although the fit was made to all elements in Table I ($9 \leq A \leq 238$) the lighter elements exerted little influence on the fit due to large uncertainties in their cross sections.

C. Molecular Attenuators

The average cross sections, $\langle\sigma\rangle$, for the molecular attenuators were computed according to Eqs. (2.8) and (2.9). Comparison was made with the expected cross sections using Eq. (2.9) with the fitted values of $\sigma_0(P)$ and $\beta(P)$ (Figs. 8 and 9) used to determine the values of σ_i. In the case of hydrogen nuclei, the neutron-proton cross sections measured in Ref. 27 were used. The agreement was good within the uncertainties quoted in the previous section. Since the predicted values are somewhat more accurate than the direct measurements on the molecular attenuators, we have not tabulated the latter. Several of the measurements are among those plotted in Fig. 7. The value of A used for the horizontal coordinate is $\langle A\rangle$ from Eq. (2.8). This represents a further useful approximation not included in the equations. It is possible to get a fairly good approximation (even with hydrogenous materials) to the average cross section by simply using $\langle A\rangle$ in the expression $\sigma_0(P)\langle A\rangle^{\beta(P)}$. If accuracy better than about 15% is required, one should evaluate the more accurate (but more tedious) expression $\sigma_0(P)\langle A^{\beta(P)}\rangle$.

ACKNOWLEDGMENTS

We are grateful to Professor M. G. White, Professor W. Wales, and the staff of the Princeton-Pennsylvania accelerator for their hospitality, help, and encouragement during this work. Dr. J. Norem helped in the design of the beam line. C. Muehleisen, R. Cuilwik, J. Fennimore, P. Cooper, I. Mayk, and S. L. Hsu helped in the construction of the apparatus. One of us (W.S.) wishes to thank Professor F. Haughey for advice and support during this work. Several of the attenuators were obtained under a grant from the American Metals Company.

---

*Work supported in part by National Science Foundation Grant Nos. GU-1592 and GP-14703, and U. S. Atomic Energy Commission Contract No. AT(30-1)-4159.

†Present address: Princeton Particle Accelerator, Physics Department, Princeton University, Princeton, New Jersey 08540.

‡Work performed in partial fulfillment of the requirements for Ph.D. degree at Rutgers University.

§Present address: MP Division, Los Alamos Scientific Laboratory, Los Alamos, New Mexico 87544.

[1]A. Ashmore, R. G. Jarvis, D. S. Mather, and S. K. Sen, Proc. Phys. Soc. (London) A70, 745 (1957).

[2]V. A. Nedzel, Phys. Rev. 94, 174 (1954).

[3]V. P. Dzhelepov, V. I. Satarov, and B. M. Golovin, Zh. Eksperim. i Teor. Fiz. 29, 369 (1955) [transl.: Soviet Phys. – JETP 2, 349 (1956)]; Doklady, Akad. Nauk SSSR 104, 717 (1955) [transl.: Lawrence Berkeley Laboratory Report No. UCRL-Trans-257, 1956 (unpublished)].

[4]N. E. Booth, G. W. Hutchinson, and B. Ledley, Proc. Phys. Soc. (London) 71, 293 (1958).

[5]T. Coor, D. A. Hill, W. F. Hornyak, L. W. Smith, and G. Snow, Phys. Rev. 98, 1369 (1955).

[6]*Neutron Cross Sections*, compiled by D. J. Hughes and R. B. Schwartz, Brookhaven National Laboratory Report No. BNL-325 (U. S. GPO, Washington, D. C.), 2nd ed., Suppl. No. 1, July, 1958; D. J. Hughes, B. A. Magurno, and M. K. Brussel, *ibid.* 2nd ed., Suppl. No. 1, January, 1960; J. R. Stehn, M. D. Goldberg, B. A. Magurno, and R. Wiener-Chasman, *ibid.* 2nd ed., Suppl. No. 2, Vol. I, $Z = 1$ to 20, May 1964, M. D. Goldberg, S. F. Mughaghab, B. A. Magurno, and V. M. May, *ibid.* 2nd ed., Suppl. No. 2, Vol. IIA, $A = 21$ to 40, February 1966; M. D. Goldberg, S. F. Mughaghab, S. N. Purohit, B. A. Magurno, and V. M. May, *ibid.* 2nd ed., Suppl.

No. 2, Vol. IIB, $Z=41$ to 60, May 1966; Vol. IIC, $Z=61$ to 87, August 1966; J. R. Stehn, M. D. Goldberg, R. Weiner-Chasman, S. F. Mughaghab, B. A. Magurno and V. M. May, *ibid.* 2nd ed. Suppl. No. 2, Vol. III, $Z=88$ to 98, February 1965. A newsletter updating this information periodically is available from the National Neutron Cross Section Center, Brookhaven National Laboratory, Upton, New York 11973.

[7]P. H. Bowen, J. P. Scanlon, G. H. Stafford, J. J. Thresher, and P. E. Hodgson, Nucl. Phys. 22, 640 (1961).

[8]R. Sherr, Phys. Rev. 68, 240 (1945).

[9]R. H. Hildebrand and E. C. Leith, Phys. Rev. 80, 842 (1950).

[10]L. J. Cook, E. M. McMillan, J. M. Peterson, and D. C. Sewell, Phys. Rev. 75, 7 (1949).

[11]D. F. Measday and J. N. Palmieri, Nucl. Phys. 85, 129 (1966).

[12]A. E. Taylor and E. Wood, Phil. Mag. 44, 95 (1953).

[13]G. R. Mott, G. L. Guernsey, and B. K. Nelson, Phys. Rev. 88, 9 (1952).

[14]J. DeJuren, Phys. Rev. 80, 27 (1950).

[15]R. Fox, C. Leith, and L. Wouters, Phys. Rev. 80, 23 (1950).

[16]W. L. Lakin, E. B. Hughes, L. H. O'Neill, and J. N. Otis, Phys. Letters 31B, 677 (1970).

[17]E. F. Parker, T. Dobrowolski, H. R. Gustafson, L. W. Jones, M. J. Longo, F. E. Ringia, and B. Cork, Phys. Letters 31B, 250 (1970).

[18]J. Engler, K. Horn, J. König, F. Mönnig, P. Schludecker, H. Schopper, P. Sievers, H. Ullrich, and K. Runge, Phys. Letters 28B, 64 (1968).

[19]J. Engler, K. Horn, F. Mönnig, P. Schludecker, W. Schmidt-Parzefall, H. Schopper, P. Sievers, H. Ullrich, R. Hartung, K. Runge, and Yu. Galaktionov, Phys. Letters 32B, 716 (1970).

[20]L. W. Jones, M. J. Longo, J. R. O'Fallon, and M. N. Kreisler, Phys. Letters 27B, 329 (1968).

[21]N. Metropolis, R. Bivins, M. Storm, A. Turkevich, J. M. Miller, and G. Friedlander, Phys. Rev. 110, 185 (1958); 110, 204 (1958).

[22]H. W. Bertini, Phys. Rev. 131, 1801 (1963); 138, AB2(E) (1965).

[23]H. W. Bertini, Oak Ridge National Laboratory Report No. ORNL-TM-1225, 1965 (unpublished); Oak Ridge National Laboratory Report No. ORNL-TM-1996, 1967 (unpublished).

[24]K. Chen, Z. Fraenkel, G. Friedlander, J. R. Grover, J. M. Miller, and Y. Shimamoto, Phys. Rev. 166, 949 (1968).

[25]R. J. Glauber, in *Lectures in Theoretical Physics*, edited by W. E. Brittin and L. G. Dunham (Interscience, New York, 1959), Vol. 1.

[26]V. Franco, Phys. Rev. Letters 24, 1452 (1970).

[27]R. E. Mischke, T. J. Devlin, W. Johnson, J. Norem, K. Vosburgh, and W. Schimmerling, Phys. Rev. Letters 25, 1724 (1970).

[28]W. Schimmerling, Ph.D. thesis, Rutgers University, 1971 (unpublished).

[29]F. F. Chen, C. P. Leavitt, and A. Shapiro, Phys. Rev. 99, 857 (1955).

[30]N. E. Booth, B. Ledley, D. Walker, and D. H. White, Proc. Phys. Soc. (London) 71, 209 (1958).

[31]G. J. Igo, J. L. Friedes, H. Palevsky, R. Sutter, G. Bennet, W. D. Simpson, D. M. Corely, and R. L. Stearns, Nucl. Phys. B3, 181 (1967).

[32]D. V. Bugg, D. C. Salter, G. H. Stafford, R. F. George, K. F. Riley, and R. J. Tapper, Phys. Rev. 146, 980 (1966).

[33]U. Amaldi, Jr., T. Fazzini, G. Fidecaro, C. Ghesquiere, M. Legros, and H. Steiner, Nuovo Cimento 34, 825 (1964).

[34]W. Galbraith, Rept. Progr. Phys. 32, 547 (1969).

[35]G. A. Sayer, E. F. Beall, T. J. Devlin, P. F. Shepard, and J. Solomon, Phys. Rev. 169, 1045 (1968).

[36]P. F. Shepard, T. J. Devlin, R. E. Mischke, and J. Solomon, Princeton University Report No. PPAR 10, 1969 (unpublished); P. Shepard, Ph.D. thesis, Princeton University, March, 1969 (unpublished).

[37]R. C. Webb, M. G. Hauser, and R. E. Mischke, Nucl. Instr. Methods 88, 227 (1970).

[38]B. R. Bevington, *Data Reduction and Error Analysis for the Physical Sciences* (McGraw-Hill, New York, 1969).

[39]G. Bellettini, G. Cocconi, A. N. Diddens, E. Lillethun, G. Matthias, J. P. Scanlon, and M. A. Wetherell, Nucl. Phys. 79, 609 (1965).

[40]W. D. Lock, *High Energy Nuclear Physics* (Methuen, London, 1960).

[41]Parametrization by R. Sievers quoted in Ref. 17.

[42]F. Solmitz, Ann. Rev. Nucl. Sci. 14, 375 (1964).

[43]W. Schimmerling, T. J. Devlin, W. Johnson, K. G. Vosburgh, and R. E. Mischke, Phys. Letters 37B, 177 (1971).

[44]H. Palevsky, J. L. Friedes, R. J. Sutter, R. E. Chrien, and H. R. Meuther, in *Proceedings of the International Congress on Nuclear Physics, Paris, France, 1962* (Centre National de la Recherche Scientifique, Paris, France, 1964), p. 162.

[45]E. F. Parker, T. Dobrowolski, H. R. Gustafson, L. W. Jones, M. J. Longo, F. E. Ringia, and B. Cork, Phys. Letters 31B, 246 (1970).

[46]J. Engler, K. Horn, J. Konig, F. Monnig, P. Schludecker, H. Schopper, P. Sievers, H. Ullrich, and K. Runge, Phys. Letters 28B, 64 (1968).

[47]L. W. Jones, M. J. Longo, T. P. McCorriston, E. F. Parker, A. J. Powell, and M. N. Kreisler, Phys. Letters 36B, 509 (1971).

[48]T. E. O. Ericson and M. P. Locher, Nucl. Phys. A148, 1 (1970).

[49]J. Pumplin and M. Ross, Phys. Rev. Letters 21, 1778 (1968).

[50]G. V. Bochman, O. Kofoed-Hansen, and B. Margolis, Phys. Letters 33B, 222 (1970).

[51]Particle Data Group, Rev. Mod. Phys. 43, S1 (1971); W. A. Wright, V. E. Anderson, J. E. Turner, J. Neufeld, and W. S. Snyder, Health Phys. 16, 13 (1969).